LIMNOLOGY AND OCEANOGRAPHY
Letters

ASLO
Open Access

Limnology and Oceanography Letters 9, 2024, 827–836

doi: 10.1002/lol2.10426

LETTER

Biologically driven isotope fractionation in ultrastructurally different shell portions of freshwater pearl mussels (*Margaritifera margaritifera*): Implications for stream water $\delta^{18}O$ reconstructions

Christoph J. Gey[1]*, *Laurent Pfister*[2,3], *Guilhem Türk*[2,3], *Frankie Thielen*[4], *Loic Leonard*[3], *Katharina E. Schmitt*[1], *Bernd R. Schöne*[1]

[1]Institute of Geosciences, University of Mainz, Mainz, Germany; [2]CAT/ENVISION/ERIN, Luxembourg Institute of Science and Technology, Belvaux, Luxembourg; [3]Faculty of Science, Technology and Medicine, University of Luxembourg, Esch-sur-Alzette, Luxembourg; [4]natur&ëmwelt Fondation Hëllef fir d'Natur, Marnach, Luxembourg

Scientific Significance Statement

Freshwater pearl mussel shells can be used to reconstruct chronicles of the oxygen isotope ($\delta^{18}O_{water}$) values of stream water, providing a novel approach to investigate multi-decadal to centennial watershed dynamics. The accuracy of such reconstructions depends on selecting the shell layer that best approximates $\delta^{18}O_{water}$, that is, determining the shell portion that is precipitated closest to oxygen isotope equilibrium with the ambient water. However, to date, no study has compared the isotope data of the two ultrastructurally distinct sublayers of the outer shell layer (i.e., outer prismatic and inner nacreous), as there was the general assumption that no difference exists. Our study uncovers biologically driven isotope fractionation mechanisms that differ between these sublayers, likely present in numerous bivalve species whose OSL consists of ultrastructurally distinct sublayers. This hitherto overlooked source of error urgently needs to be addressed in isotope-based environmental reconstructions with bivalves in both freshwater and marine settings.

Abstract

Oxygen isotopes in stream water can serve as natural tracers of watershed dynamics. Freshwater pearl mussels provide $\delta^{18}O_{water}$ estimates that overcome temporal and spatial limitations of instrumental records. The reliability of shell-based $\delta^{18}O_{water}$ reconstructions depends on understanding which shell layer biomineralizes closer to oxygen isotopic equilibrium with ambient water. To determine this, both the (outer) prismatic and (inner) nacreous sublayers of the outer shell layer were sampled. Over 2500 isotope values were obtained from shells collected from the Our River (Luxembourg) and from mussels cultured in tanks at constant temperature and

*Correspondence: christoph.gey@uni-mainz.de

Associate editor: Clive Trueman

Author Contribution Statement: CJG: Formal analysis and investigation of shell isotopes, Validation, Methodology, Visualization, Writing – original draft. LP: Project administration, Funding acquisition, Supervision, Writing – review & editing. GT: Sampling and investigation of water isotopes, Writing – review & editing. FT: Management of tank experiments, Methodology, Writing – review & editing. LL: Measurement and investigation of water isotopes, Writing – review & editing. KES: Investigation of shell isotopes, Visualization, Writing – review & editing. BRS: Resources, Conceptualization, Formal analysis, Investigation, Validation, Supervision, Project administration, Funding acquisition, Writing – original draft, Writing – review & editing.

Data Availability Statement: Data are available in the Zenodo data repository at DOI https://doi.org/10.5281/zenodo.11082703.

Additional Supporting Information may be found in the online version of this article.

monitored $\delta^{18}O_{water}$. Calculated $\delta^{18}O_{water}$ from the prismatic portion was in excellent agreement with monitored $\delta^{18}O_{water}$, while $\delta^{18}O_{shell}$ of the nacreous portion was systematically offset by +0.43‰, overestimating $\delta^{18}O_{water}$ by +0.53‰. Although shell portions were formed simultaneously from the same extrapallial fluid, they underwent different fractionation mechanisms, presumably due to differences in carbonic anhydrase activity catalyzing mineralization processes.

Oxygen isotopes in stream water ($\delta^{18}O_{water}$) can provide valuable information about water sources, flow paths, and transit times (*see* review by Klaus and McDonnell 2013). However, instrumental $\delta^{18}O_{water}$ records have limited temporal and spatial coverage and barely cover more than a few decades (Halder et al. 2015). Bivalve shells, which are precipitated near oxygen isotope equilibrium with ambient water, have been investigated to complement these records (Versteegh et al. 2010; Kelemen et al. 2017; Pfister et al. 2019). Of particular interest are long-lived species such as the freshwater pearl mussel (FPM), *Margaritifera margaritifera*. With lifespans of over 200 yr (Mutvei and Westermark 2001), it is an ideal candidate for reconstructing uninterrupted, high-resolution, multi-decadal to multi-centennial $\delta^{18}O_{water}$ records (Pfister et al. 2018; Schöne et al. 2020). The accuracy of such reconstructions relies on the evaluation and selection of the shell portion that closely reflects $\delta^{18}O_{water}$.

Like other bivalves, FPM shells consist of a layered structure with an outer shell layer (OSL) and an inner shell layer (ISL) (Dunca 1999). Biomineralization of these two layers takes place in the outer and inner extrapallial spaces (oEPS and iEPS), narrow spaces (< 100 nm) between the mantle epithelia and the forming shell (Nakahara and Bevelander 1971; Checa 2000, 2018). The extrapallial spaces are filled with an extrapallial fluid or gel (EPF) (Cartwright and Checa 2007). Through the EPF, the mineralization front of the shell is supplied with $CaCO_3$ precursors and organic macromolecules (*see* review by Marin et al. 2012). These macromolecules, largely polysaccharides and proteins, are synthesized by the mantle epithelium and form a soluble organic matrix that acts as scaffolding for the aragonitic mineral phase (Cartwright and Checa 2007). The $CaCO_3$ precursors (CO_2, HCO_3^-, CO_3^{2-}, and Ca^{2+}) can be derived from two sources: dissolved inorganic carbonate (DIC) from the surrounding water (eDIC) or DIC from metabolic processes (mDIC) (Curley et al. 2023). When reconstructing environmental parameters, the focus is typically on the isotopic composition of the OSL because it is less affected by mDIC and, thus, closer to isotopic equilibrium with the surrounding water (McConnaughey and Gillikin 2008; Curley et al. 2023). In FPM shells, the OSL is composed of two aragonitic, ultrastructurally (= microstructurally) different portions: a prismatic outer sublayer (= oOSL) and a nacreous inner sublayer (= iOSL) (Dunca 1999). Both portions show contiguous annual growth lines, indicating that they formed simultaneously with DIC species originating from the same oEPF.

Recent isotope studies on FPM primarily focused on the oOSL (Pfister et al. 2018; Schöne et al. 2020). However, the use of this portion comes with the disadvantage that it is prone to dissolution, leading to the natural loss of the first 5–10 ontogenetic years and occasional gaps within the record. Such susceptibility of the outermost shell portion to dissolution, as well as potential diagenetic alterations, pose a common challenge in sclerochronological studies involving fossils (e.g., Cochran et al. 2010) and long-lived recent organisms (e.g., Casella et al. 2017). Consequently, sampling is often conducted at the best-preserved shell portion, irrespective of verification for isotopic equilibrium formation. Actually, studies examining isotopic differences among ultrastructurally distinct portions of the shell are scarce (e.g., Geist et al. 2005; Trofimova et al. 2018; Curley et al. 2023). Trofimova et al. (2018) have recently shown that the ocean quahog, *Arctica islandica*, a marine bivalve inhabiting the northern North Atlantic, exhibits systematic differences in the isotopic composition between the two sublayers of the OSL, where the iOSL showed an ^{18}O enrichment resulting in 0.46‰ higher $\delta^{18}O_{shell}$ values than the oOSL, although both sublayers were composed of aragonite and formed contemporaneously from the same oEPF. The study by Trofimova et al. (2018) did not include a comparison with $\delta^{18}O_{water}$ measured in situ to determine which shell portion was closer to equilibrium. Yet, they demonstrated that temperatures reconstructed from $\delta^{18}O_{shell}$ of the oOSL are in better agreement with instrumental temperature data. The cause of this phenomenon remains unknown. According to Trofimova et al. (2018), the offset could be attributed to fractionation induced by heat generated during micromilling (Waite and Swart 2015). Alternatively, it may have resulted from dissolution by acidic metabolites as proposed by Crenshaw and Neff (1969) or by poorly understood biochemical effects during biomineralization. In particular, the latter would have unpredictable effects on various chemical properties, with significant implications for bivalve-based paleoenvironmental reconstructions. Consequently, finding the origin of this phenomenon has been considered as one of the fundamental questions in the research priorities defined by the sclerochronology community in 2020 (Trofimova et al. 2020).

In this study, we investigated differences in isotopic composition ($\delta^{18}O$ and $\delta^{13}C$) between the iOSL and oOSL of the FPM. To determine the shell portion closest to oxygen isotope equilibrium with ambient water, we analyzed $\delta^{18}O_{shell}$ of juvenile specimens cultured in tanks with monitored $\delta^{18}O_{water}$. In addition, we used adult mussels (up to 48 yr-old) collected from the Our River in Luxembourg to study isotope variability on a multi-decadal time scale with a seasonal resolution. The

results of our study contribute significantly to the reliability of *M. margaritifera* as $\delta^{18}O_{water}$ archive. In addition, it provides evidence for biomineralization processes that lead to isotopic fractionation. These insights are critical for advancing bivalve-based environmental reconstructions, given their occurrence in different species.

Material and methods

Shells of three adult FPM (D1, D3, and D4) were collected from the Our River, west of the village Kalborn (KAL), in June 2013 (Table 1). Mussels were found dead but articulated, with only partially decayed soft tissues, indicating that the animals had died shortly before collection. In addition, juvenile specimens were reared over 2 yr in tanks at the Kalborn Mill mussel breeding station in Luxembourg, operated by the Fondation Hëllef fir d'Natur by "natur&ëmwelt." Tanks were maintained at constant temperatures of 10°C, 14°C, 18°C, and 22°C (for detailed experimental setup, *see* Gey et al. 2023). From each temperature regime, five shells were used for isotope analyses, with permission granted by the Ministère de l'Environnement, du Climat et du Développement Durable (authorization reference number 98405 GB/sr).

Isotope analysis

For isotope analysis of the shells, all mussels were prepared using established sclerochronological methods (Supporting Information). Powder samples were milled from both OSL sublayers. The sampling protocol (Supporting Information) ensured the optimal alignment of corresponding isotope values from oOSL and iOSL of the same annual increment and prevented cross-contamination between the different shell portions.

Powder samples were measured with a Thermo Fisher MAT 253 isotope ratio mass spectrometer coupled to a GasBench II (for details, *see* Supporting Information). Results were presented in δ-notation relative to the Vienna Pee Dee Belemnite (VPDB). Reported $\delta^{18}O_{shell}$ values were not adjusted for differences in acid fractionation factors of different polymorphs of $CaCO_3$ (Füllenbach et al. 2015).

To determine the $\delta^{18}O_{water}$ from the $\delta^{18}O_{shell}$, the empirical equation by Grossman and Ku (1986) was solved for $\delta^{18}O_{water}$ as described in Schöne et al. (2020) (Eq. 1), including the correction for the VPDB–VSMOW scale difference by Gonfiantini et al. (1995).

$$\delta^{18}O_{water} = \frac{19.43 - 4.34 \times \delta^{18}O_{shell} - T_{water}}{-4.34} \quad (1)$$

Table 1. List of field-grown and tank-grown specimens of *Margaritifera margaritifera* shells used in the present study. The character of specimen ID following the hyphen indicates if the bivalve was collected alive (A) or was found dead (D). Due to umbonal corrosion, the first 5–10 yr of field-grown specimens are typically missing and the listed age thus represents a minimum estimate based on annual growth increment counts.

Field-grown specimens

					# Isotope samples	
Stream, country	Specimen ID	Coordinates	Age (yr)	Covered time interval (yr C.E.)	oOSL	iOSL
Our, Luxembourg	2021-KAL-D1	50°06′07.79″N, 006°07′54.96″E	48	1964–2012	433	349
	2021-KAL-D3		26	1986–2012	267	452
	2021-KAL-D4		46	1966–2012	467	477

Tank-grown specimens

			# Isotope samples					# Isotope samples	
Specimen ID	Temp. (°C)	Age (yr)	oOSL	iOSL	Specimen ID	Temp. (°C)	Age (yr)	oOSL	iOSL
10-A1	10	1	17	n.a.	18-A1	18	1	33	2
10-A2		1	6	5	18-A2		1	18	14
10-A3		1	9	7	18-A3		1	15	7
10-D9		2	5	3	18-D20		2	9	6
10-D19		2	8	n.a.	18-D32		2	3	n.a.
14-A1	14	1	21	5	22-A1	22	1	49	n.a.
14-A2		1	11	8	22-A2		1	16	14
14-A3		1	8	7	22-A3		1	16	17
14-D10		2	8	8	22-D12		2	22	20
14-D14		2	10	n.a					

For in situ $\delta^{18}O_{water}$ measurements in the tanks, water samples were collected at 2- to 3-d intervals and analyzed with a Los Gatos Research Liquid Water Isotope Analyzer LGR LWIA-24d with a measurement precision of 0.20‰. The complete data set of the isotope values from water and shells is openly available in the Zenodo data repository (Gey et al. 2024).

Temporal alignment of shell isotope data from field specimens

To improve the visibility of annual growth lines, a 2-mm thick section of each shell was immersed in Mutvei's solution (Schöne et al. 2005) (Fig. 1a), and the width of the annual increments measured as described by Dunca et al. (2005) (Supporting Information). To place each isotope sample in a seasonal context, we temporally aligned the isotope samples of the oOSL using a refined version of the growth model from Gey et al. (2023) (Supporting Information). This model relates shell growth to water temperature, with increased growth in summer and decreased growth in spring, fall, and winter. Samples collected within the first 11% of the annual increment after a winter line corresponded to May, while those between 11% and 31% were assigned to June, 31% to 59% to July, 59% to 85% to August, and the final 15% before the next annual growth line to September (Fig. 1a,c). In dyed shell sections, winter and intra-annual growth lines can be traced continuously from the oOSL to the iOSL, confirming the contemporaneous formation of both sublayers. However, in unstained sections used for micromilling, the visibility of intra-annual growth patterns in the nacreous iOSL is reduced. To address this, we used dynamic time warping (DTW) to synchronize the isotope values of the iOSL with the temporally aligned oOSL (Supporting Information). DTW compares two series by measuring the distance between each value in one series to all values in the other series (Wang and Gasser 1997). These distances are stored in a cost matrix (Fig. 1b), which represents the distance between each point. The algorithm originally developed by Sakoe and Chiba (1978) finds the best alignment path that has the minimal cumulative distance in the cost matrix (Fig. 1b,c).

Results

To determine the quality of how well each shell portion reflects $\delta^{18}O_{water}$, 407 powder samples of tank-reared

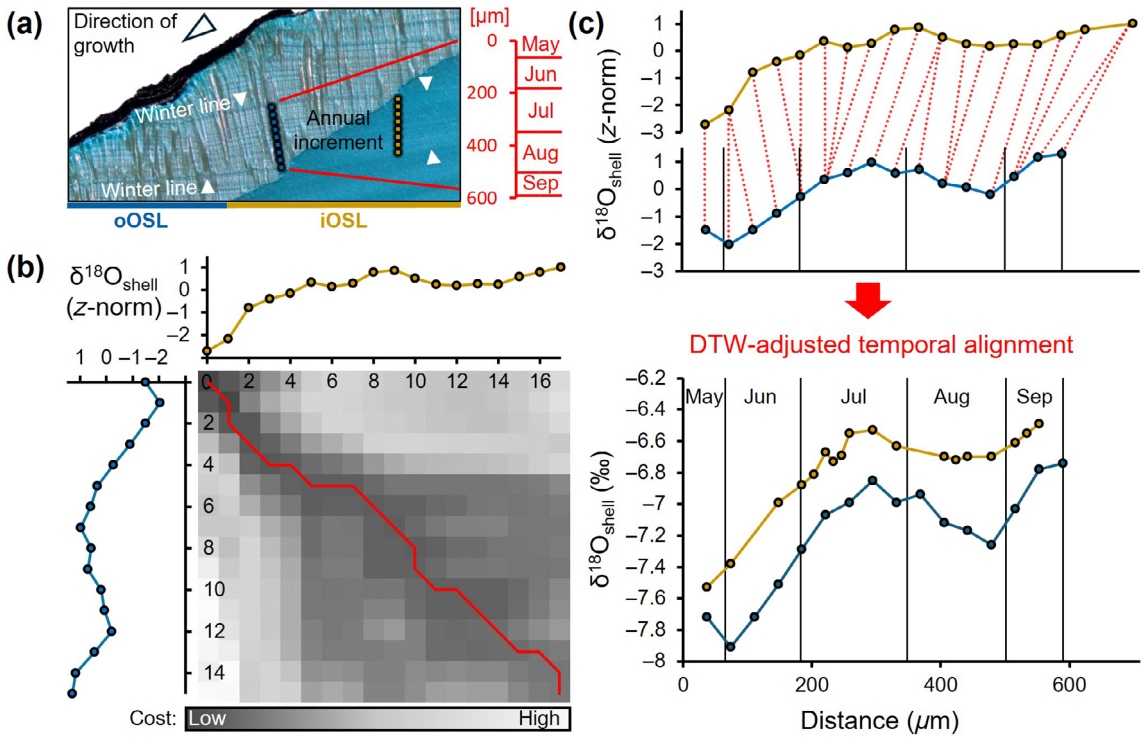

Fig. 1. Illustration of the temporal alignment of isotope samples using a tank-derived growth model and dynamic time warping (DTW). (**a**) Shell section immersed in Mutvei's solution showing the outer shell layer (OSL) with the isotope sampling paths (dotted lines) in the two contemporaneously formed sections of the outer (oOSL) and inner portion (iOSL). The red graph illustrates the seasonal growth of the oOSL over the year based on a tank-derived growth model. (**b**) DTW approach for aligning iOSL to oOSL isotope values, showing the cost matrix between *z*-normalized $\delta^{18}O_{shell}$ values of both sublayers. The best alignment path is determined by the lowest cumulative cost in the matrix (red line). (**c**) Top: *Z*-normalized $\delta^{18}O_{shell}$ chronology with temporally aligned oOSL values via tank-based monthly growth model; iOSL values connected to corresponding oOSL values via DTW alignment (red dashed lines). Bottom: Final DTW-adjusted $\delta^{18}O_{shell}$ timeseries of both shell portions.

specimens were compared to 581 in situ $\delta^{18}O_{water}$ measurements made over 1 yr. Isotope records of the three adult specimens spanned from 1964 to 2013 and included 2445 $\delta^{18}O$ and $\delta^{13}C$ data, providing insights into the seasonal and long-term covariance of the isotopic composition between oOSL and iOSL.

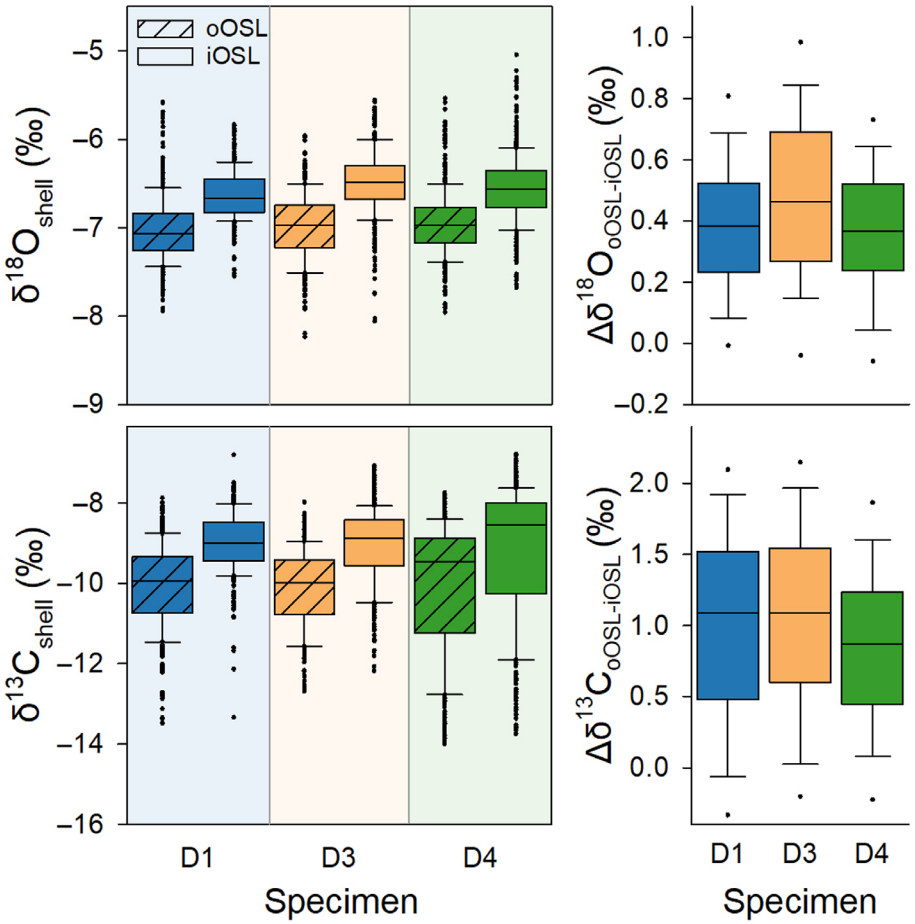

Fig. 2. Stable oxygen ($\delta^{18}O$) and carbon ($\delta^{13}C$) isotope values of the outer portion (oOSL) and inner portion (iOSL) of the outer shell layer in three specimens of *Margaritifera margaritifera* collected in the Our River at Kalborn Mill, Luxembourg in 2013. Box plots with medians and interquartiles.

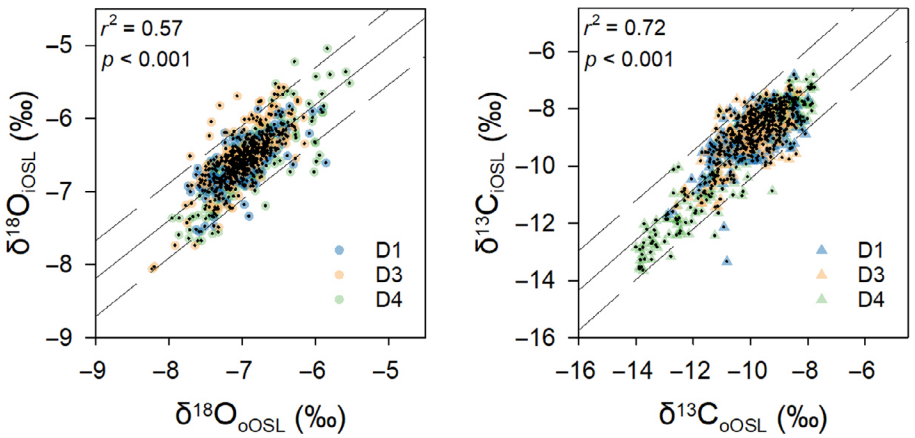

Fig. 3. Relationship between the stable oxygen ($\delta^{18}O$) and carbon ($\delta^{13}C$) isotope values of the outer and inner portion of the outer shell layer (oOSL and iOSL, respectively) of three *Margaritifera margaritifera* specimens from the Our River. The linear regression lines (solid) with 95% confidence bands (dashed) are displayed. Temporal alignment was achieved using a seasonal growth model on the oOSL, and dynamic time warping (DTW) was applied to align the oOSL and iOSL isotopes.

Monitored vs. reconstructed $\delta^{18}O_{water}$ in tank specimens

Applying Eq. 1, the $\delta^{18}O_{shell}$-derived $\delta^{18}O_{water}$ values of the oOSL showed a higher agreement with in situ $\delta^{18}O_{water}$ than reconstructions from the iOSL (Supporting Information Fig. S2). In particular, the average offset of $\delta^{18}O_{water(oOSL)}$ of +0.26‰ only slightly exceeded the measurement precision of the water isotope analysis, whereas $\delta^{18}O_{water(iOSL)}$ was on average +0.53‰ higher than the instrumental $\delta^{18}O_{water}$. Notably, with increasing temperature, the offset between $\delta^{18}O_{water(iOSL)}$ and in situ $\delta^{18}O_{water}$ increased. Specifically, the median of $\delta^{18}O_{water(iOSL)}$ in the 10°C tank corresponded exactly to the in situ measurement, but gradually increased noticeably in the 14°C, 18°C, and 22°C tanks with offsets of +0.48‰, +0.79‰, and +0.86‰, respectively.

Isotope patterns in field-grown specimens: Comparison across shell sublayers

The $\delta^{18}O_{shell}$ of the adult mussels from Our River ranged from −8.24‰ to −5.05‰ with a median of −6.77‰ and an interquartile range (IQR) of 0.57‰ (Fig. 2). We found a high agreement in $\delta^{18}O_{shell}$ among the specimens, but significant differences between the two shell portions (Wilcoxon signed-rank test, $Z = 21.1$; $p < 0.001$, $r = 0.8$). Notably, all three specimens exhibited higher $\delta^{18}O_{shell}$ values in the iOSL ($\delta^{18}O_{iOSL}$),

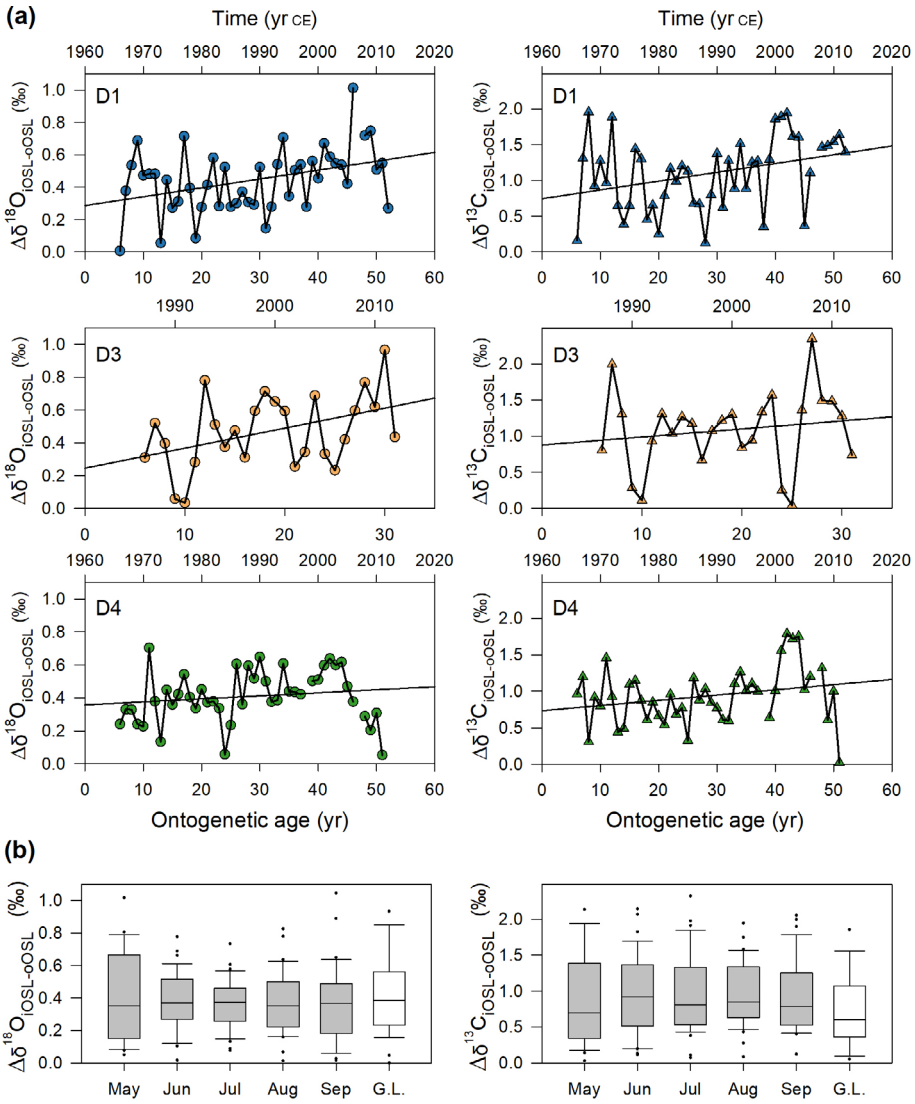

Fig. 4. Plot showing the relationship between oxygen and carbon isotope offsets between the different shell portions ($\Delta\delta^{18}O_{iOSL\text{-}oOSL}$; $\delta^{13}C_{iOSL\text{-}oOSL}$) of *Margaritifera margaritifera* on (**a**) interannual and (**b**) seasonal time scales. (**a**) Interannual evolution of the offsets with ontogenetic age (*x*-axis 1) and calendar year C.E. (*x*-axis 2). (**b**) Monthly isotope offsets are shown in boxplots with medians and quartiles. Box labeled G.L. shows offsets of isotope values of an annual growth line that cannot be clearly assigned to the end of the growing season or the beginning of the next growing season. Boxplots include only years with sufficient resolution in which, in both shell layers, all months of the growing season were represented.

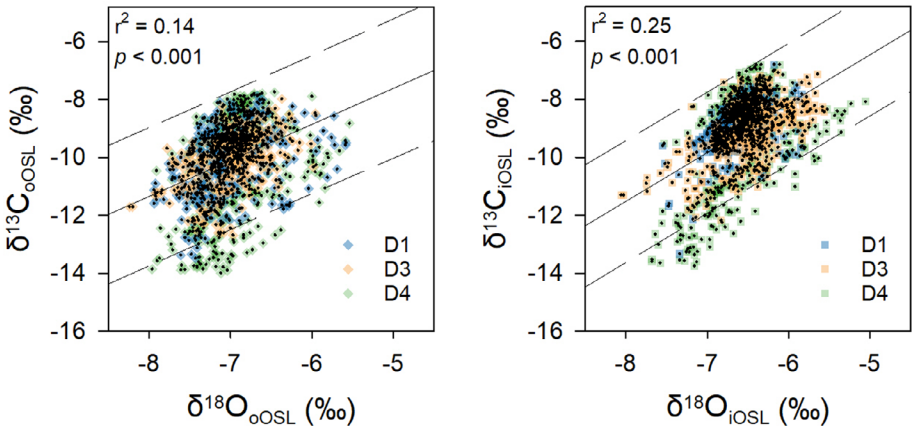

Fig. 5. Correlation between oxygen ($\delta^{18}O$) and carbon ($\delta^{18}C$) isotope values in the oOSL (left) and iOSL (right) of three *Margaritifera margaritifera* specimens from the Our River. The linear regression lines (solid) and prediction bands (dashed) are displayed.

with an average offset of +0.43‰ from the oOSL ($\delta^{18}O_{oOSL}$), albeit there was a positive correlation between $\delta^{18}O_{shell}$ values of the two shell layers ($r^2 = 0.57$; $p < 0.001$) (Fig. 3). A similar pattern was observed in stable carbon isotopes, with $\delta^{13}C_{iOSL}$ was 1.00‰ higher than $\delta^{13}C_{oOSL}$, while data from both sublayers were positively correlated ($r^2 = 0.72$; $p < 0.001$).

Both offsets, $\Delta\delta^{18}O_{iOSL\text{-}oOSL}$ and $\Delta\delta^{13}C_{iOSL\text{-}oOSL}$, showed strong interannual variation in all studied adult shells (Fig. 4a), but no significant correlation was found with either the ontogenetic age of the mussel or the calendar year. On an intra-annual scale (Fig. 4b), no significant differences existed for either $\Delta\delta^{18}O_{iOSL\text{-}oOSL}$ (Kruskal–Wallis; $p = 0.979$) or $\Delta\delta^{13}C_{iOSL\text{-}oOSL}$ ($p = 0.351$). However, in every shell, we found a distinct relationship between $\Delta\delta^{18}O_{iOSL\text{-}oOSL}$ and $\Delta\delta^{13}C_{iOSL\text{-}oOSL}$, with D1: $r^2 = 0.31$; D3: $r^2 = 0.41$ and D4: $r^2 = 0.36$ ($p < 0.001$).

Furthermore, in both shell portions, significant correlations existed between $\delta^{18}O$ and $\delta^{13}C$ (Fig. 5). Notably, this relationship was higher in the iOSL ($r^2 = 0.25$) than in the oOSL ($r^2 = 0.14$). The strength of the correlations was characterized by strong seasonal variations in both oOSL and iOSL. In the outer sublayer of the OSL, a relationship between $\delta^{18}O$ and $\delta^{13}C$ was only evident in June ($r^2 = 0.21$) and July ($r^2 = 0.27$), while no significant correlation was observed at the beginning (May) and end of the main growing season (from August onward). Likewise, the iOSL showed the strongest correlation between $\delta^{18}O$ and $\delta^{13}C$ in June and July, with $r^2 = 0.35$ and $r^2 = 0.48$, respectively. Yet, the iOSL also showed a significant relationship near the winter line ($r^2 = 0.31$), that is, at the beginning of the growing season in May ($r^2 = 0.22$) and close to the end of August ($r^2 = 0.18$).

Discussion

In tank specimens, $\delta^{18}O_{water}$ data reconstructed from the oOSL was in excellent agreement with instrumental $\delta^{18}O_{water}$ values, while the $\delta^{18}O_{shell}$ of the iOSL was systematically offset by +0.43‰, resulting in an overestimation of $\delta^{18}O_{water}$ by +0.53‰. This difference contradicts the assumption that simultaneous formation from the same EPF results in identical isotope compositions. The following discussion explores the possible causes and addresses the implications of these differences for isotope-based environmental reconstructions.

Origin of isotopic disequilibria during biomineralization

The isotope offset between shell portions existed for oxygen ($\Delta\delta^{18}O_{iOSL\text{-}oOSL} = 0.43‰$) and carbon ($\Delta\delta^{13}C_{oOSL\text{-}iOSL} = 1.00‰$), pointing to a common fractionation mechanism for both elements as a result of kinetic effects (Owen et al. 2002). Kinetic effects can occur during the reactions of CO_2 hydration/HCO_3^- dehydration and CO_2 hydroxylation/HCO_3^- dehydroxylation (Sade and Halevy 2017). Both reactions are slower for molecules enriched in heavier isotopes (^{13}C and ^{18}O). If the reaction of HCO_3^- with calcium ions (Ca^{2+}) is more rapid than the required equilibration time for all oxygen and carbon isotopes, biominerals will exhibit isotopic offsets from the expected $\delta^{18}O$ and $\delta^{13}C$ values under equilibrium fractionation. The strength of the correlation between $\delta^{18}O$ and $\delta^{13}C$ can indicate the strength of such a fractionation (Keith and Weber 1965; McConnaughey 1989; Chen et al. 2018). In the present study, $\delta^{18}O$ and $\delta^{13}C$ were correlated in both OSL sublayers of all three studied field-grown specimens. The correlation strength showed strong seasonal variability, with peaks in June (oOSL $r^2 = 0.21$, iOSL $r^2 = 0.35$) and July (oOSL: $r^2 = 0.27$; iOSL: $r^2 = 0.48$). This coincides with the period of faster shell growth rates, supporting the hypothesis that kinetic effects are at work. Although the correlation could also originate from natural seasonal changes of $\delta^{18}O$ and $\delta^{13}C$ in the water, it cannot explain that the strength of this correlation not only varied seasonally, but also between the two OSL sublayers (oOSL: $r^2 = 0.14$; iOSL: $r^2 = 0.25$). Both portions were formed from the same EPF, originating from an identical pool of precursor ions and being exposed to similar

pH and temperature conditions. Consequently, we would expect identical kinetic isotope fractionations for both portions due to the same (de)hydration/(de)hydroxylation rates and equilibration times, given that the EPF is not differentially fractionated at the cellular level. However, this was not observed in the tanks, where the iOSL showed an increasing offset from the instrumental $\delta^{18}O_{water}$ with rising water temperatures, a trend not seen in the oOSL.

The reason why the shell portions were unequally susceptible to kinetic fractionation may lie in the activity of carbonic anhydrase (CA). Proteins with CA domains are present in many calcifying organisms (Evans 2019). In bivalves, they are a component of the soluble organic matrix and play an essential role in the regulation of biomineralization processes, particularly in catalyzing the CO_2 (de)hydration/(de)hydroxylation (McConnaughey 1989). Proteomic analyses have shown that the abundance and types of these proteins vary between nacreous and prismatic ultrastructures (Liao et al. 2015; Namikawa et al. 2023). A kinetic model of biomineralization by Chen et al. (2018) proposed that variations in CA activity could explain differing slopes of $\delta^{18}O$ vs. $\delta^{13}C$ among various calcifying organisms. This is because oxygen isotopes take longer (hours to days) to equilibrate than carbon isotopes (seconds to minutes) (Zeebe and Wolf-Gladrow 2001). Thus, an enhancement of (de)hydration/(de)hydroxylation reactions by CA would change the slope between $\delta^{18}O$ and $\delta^{13}C$. The observation that the nacreous portion of all examined specimens has a systematically steeper slope (1.68) than the prismatic portion (1.25) suggests that the same mechanism may be operating in different shell portions of FPM. In addition, higher proteomic content of the nacreous portion would demand the higher energetic cost of formation for the mussel, which could also affect the relative calcification rate and time for isotopic equilibration.

Implication for paleoenvironment reconstructions

Although the $\delta^{18}O_{oOSL}$ of FPM provides superior $\delta^{18}O_{water}$ estimates, 57% of the variability is shared with $\delta^{18}O_{iOSL}$. By using the linear relationship between the $\delta^{18}O$ values of the two shell portions (Fig. 3), Eq. 1 can be adjusted for $\delta^{18}O_{iOSL}$ as follows:

$$\delta^{18}O_{water} = \frac{19.43 - 4.34 \times \left(-2.211 + \left(0.723 \times \delta^{18}O_{iOSL}\right)\right) - T_{water}}{-4.34} \quad (2)$$

This modified equation allows us to obtain serviceable $\delta^{18}O_{water}$ estimates from $\delta^{18}O_{iOSL}$ and to fill gaps in the isotope record of the oOSL, which is exposed to exterior water and, therefore, more susceptible to dissolution. Yet, reconstructions from $\delta^{18}O_{iOSL}$ with intra-annual resolution should account for appropriate uncertainties due to the kinetic effects that fluctuate seasonally.

The reported isotope offset of oxygen and carbon between different ultrastructures in FPM shells is a hitherto overlooked weakness of isotope-based environmental reconstructions. This phenomenon, presumably caused by differences in CA activity, may be present in many bivalve species whose OSL consists of ultrastructurally distinct sublayers and would explain the similar finding of Trofimova et al. (2018) in the shells of *A. islandica*. CA activity combined with mild alkalinization rates, both accelerating the isotopic equilibration, is one of the argued reasons that bivalves are generally considered to be less susceptible to kinetic effects (McConnaughey and Gillikin 2008). However, the evidence reported here for kinetics of varying strength between shell portions and of seasonally varying intensity requires attention because these have implications not only for the reconstruction of stream water $\delta^{18}O$, but also for the more widespread application of $\delta^{18}O$ thermometry (e.g., Mook and Vogel 1968; Wefer and Berger 1991; Featherstone et al. 2020) and the rapidly growing field of carbonate clumped isotope thermometry (e.g., Henkes et al. 2013; de Winter et al. 2021, 2022; Huyghe et al. 2022). In particular, Δ_{47} thermometry, which assesses the clumping of ^{13}C and ^{18}O isotopes, is highly sensitive to kinetic effects. For example, temperature reconstructions on brachiopods and both cold- and warmwater corals have shown that kinetics associated with (de)hydration/(de)hydroxylation led to very strong underestimates of the actual growth temperatures of up to 22°C (Bajnai et al. 2018, 2020). Therefore, we highly recommend performing layer-specific sampling and evaluating the portion that is not or less affected by kinetic effects. When working with fossil specimens, that renders an evaluation by comparing with monitoring data difficult, the use of dual clumped isotopes (Δ_{47} vs. Δ_{48}) can help to identify a kinetic departure from isotopic equilibrium (Davies et al. 2022). When working with contemporary samples, there is also often a lack of isotope monitoring data. In such cases, we propose to use the covariance between $\delta^{18}O$ and $\delta^{13}C$, both routinely measured simultaneously in IRMS analyses, as a first indicator to identify the portion affected by kinetic effects.

References

Bajnai, D., and others. 2018. Assessing kinetic fractionation in brachiopod calcite using clumped isotopes. Sci. Rep. **8**: 533. doi:10.1038/s41598-017-17353-7

Bajnai, D., and others. 2020. Dual clumped isotope thermometry resolves kinetic biases in carbonate formation temperatures. Nat. Commun. **11**: 4005. doi:10.1038/s41467-020-17501-0

Cartwright, J. H. E., and A. G. Checa. 2007. The dynamics of nacre self-assembly. J. R. Soc. Interface **4**: 491–504. doi:10.1098/rsif.2006.0188

Casella, L. A., and others. 2017. Experimental diagenesis: Insights into aragonite to calcite transformation of *Arctica*

islandica shells by hydrothermal treatment. Biogeosciences **14**: 1461–1492. doi:10.5194/bg-14-1461-2017

Checa, A. 2000. A new model for periostracum and shell formation in *Unionidae* (Bivalvia, Mollusca). Tissue Cell **32**: 405–416. doi:10.1054/tice.2000.0129

Checa, A. G. 2018. Physical and biological determinants of the fabrication of molluscan shell microstructures. Front. Mar. Sci. **5**: 353. doi:10.3389/fmars.2018.00353

Chen, S., A. C. Gagnon, and J. F. Adkins. 2018. Carbonic anhydrase, coral calcification and a new model of stable isotope vital effects. Geochim. Cosmochim. Acta **236**: 179–197. doi:10.1016/j.gca.2018.02.032

Cochran, J. K., K. Kallenberg, N. H. Landman, P. J. Harries, D. Weinreb, K. K. Turekian, A. J. Beck, and W. A. Cobban. 2010. Effect of diagenesis on the Sr, O, and C isotope composition of late Cretaceous mollusks from the western interior seaway of North America. Am. J. Sci. **310**: 69–88. doi:10.2475/02.2010.01

Crenshaw, M. A., and J. M. Neff. 1969. Decalcification at the mantle-shell interface in molluscs. Am. Zool. **9**: 881–885. doi:10.1093/icb/9.3.881

Curley, A. N., S. V. Petersen, S. M. Edie, and W. Guo. 2023. Biologically driven isotopic fractionations in bivalves: From palaeoenvironmental problem to palaeophysiological proxy. Biol. Rev. **98**: 1016–1032. doi:10.1111/brv.12940

Davies, A. J., W. Guo, M. Bernecker, M. Tagliavento, J. Raddatz, E. Gischler, S. Flögel, and J. Fiebig. 2022. Dual clumped isotope thermometry of coral carbonate. Geochim. Cosmochim. Acta **338**: 66–78. doi:10.1016/j.gca.2022.10.015

de Winter, N. J., R. Witbaard, I. J. Kocken, I. A. Müller, J. Guo, B. Goudsmit, and M. Ziegler. 2022. Temperature dependence of clumped isotopes (Δ_{47}) in aragonite. Geophys. Res. Lett. **49**: e2022GL099479. doi:10.1029/2022GL099479

de Winter, N. J., and others. 2021. Absolute seasonal temperature estimates from clumped isotopes in bivalve shells suggest warm and variable greenhouse climate. Commun. Earth Environ. **2**: 121. doi:10.1038/s43247-021-00193-9

Dunca, E. 1999. Bivalve shells as archives for changes in water environment. Vatten **55**: 279–290.

Dunca, E., B. R. Schöne, and H. Mutvei. 2005. Freshwater bivalves tell of past climates: But how clearly do shells from polluted rivers speak? Palaeogeogr. Palaeoclimatol. Palaeoecol. **228**: 43–57. doi:10.1016/j.palaeo.2005.03.050

Evans, J. S. 2019. The biomineralization proteome: Protein complexity for a complex bioceramic assembly process. Proteomics **19**: 1900036. doi:10.1002/pmic.201900036

Featherstone, A. M., P. G. Butler, B. R. Schöne, M. Peharda, and J. Thébault. 2020. A 45-year sub-annual reconstruction of seawater temperature in the Bay of Brest, France, using the shell oxygen isotope composition of the bivalve *Glycymeris glycymeris*. Holocene **30**: 3–12. doi:10.1177/0959683619865592

Füllenbach, C. S., B. R. Schöne, and R. Mertz-Kraus. 2015. Strontium/lithium ratio in aragonitic shells of *Cerastoderma edule* (Bivalvia)—A new potential temperature proxy for brackish environments. Chem. Geol. **417**: 341–355. doi:10.1016/j.chemgeo.2015.10.030

Geist, J., K. Auerswald, and A. Boom. 2005. Stable carbon isotopes in freshwater mussel shells: Environmental record or marker for metabolic activity? Geochim. Cosmochim. Acta **69**: 3545–3554. doi:10.1016/j.gca.2005.03.010

Gey, C. J., F. Thielen, L. Pfister, C. Hissler, G. Türk, S. Baier, and B. R. Schöne. 2023. Disturbed by pH? Nacre tablet thickness of freshwater pearl mussels (*Margaritifera margaritifera*) is a poor temperature proxy. Mar. Freshw. Res. **74**: 1129–1144. doi:10.1071/MF23058

Gey, C. J., L. Pfister, G. Türk, F. Thielen, L. Leonard, K. E. Schmitt, and B. R. Schöne. 2024. Dataset: Stable oxygen and carbon isotopes in freshwater pearl mussels from ultrastructurally distinct shell portions. Zenodo: 2024. doi:10.5281/zenodo.11082703

Gonfiantini, R., W. Stichler, and K. Rozanski. 1995. Standards and intercomparison materials distributed by the International Atomic Energy Agency for stable isotope measurements (IAEA-TECDOC825), International Atomic Energy Agency (IAEA). https://www-pub.iaea.org/MTCD/publications/PDF/te_825_prn.pdf

Grossman, E. L., and T.-L. Ku. 1986. Oxygen and carbon isotope fractionation in biogenic aragonite: Temperature effects. Chem. Geol. **59**: 59–74. doi:10.1016/0168-9622(86)90057-6

Halder, J., S. Terzer, L. I. Wassenaar, L. J. Araguás-Araguás, and P. K. Aggarwal. 2015. The Global Network of Isotopes in Rivers (GNIR): Integration of water isotopes in watershed observation and riverine research. Hydrol. Earth Syst. Sci. **19**: 3419–3431. doi:10.5194/hess-19-3419-2015

Henkes, G. A., B. H. Passey, A. D. Wanamaker, E. L. Grossman, W. G. Ambrose, and M. L. Carroll. 2013. Carbonate clumped isotope compositions of modern marine mollusk and brachiopod shells. Geochim. Cosmochim. Acta **106**: 307–325. doi:10.1016/j.gca.2012.12.020

Huyghe, D., M. Daëron, M. de Rafelis, D. Blamart, M. Sébilo, Y.-M. Paulet, and F. Lartaud. 2022. Clumped isotopes in modern marine bivalves. Geochim. Cosmochim. Acta **316**: 41–58. doi:10.1016/j.gca.2021.09.019

Keith, M. L., and J. N. Weber. 1965. Systematic relationships between carbon and oxygen isotopes in carbonates deposited by modern corals and algae. Science **150**: 498–501. doi:10.1126/science.150.3695.498

Kelemen, Z., and others. 2017. Calibration of hydroclimate proxies in freshwater bivalve shells from Central and West Africa. Geochim. Cosmochim. Acta **208**: 41–62. doi:10.1016/j.gca.2017.03.025

Klaus, J., and J. J. McDonnell. 2013. Hydrograph separation using stable isotopes: Review and evaluation. J. Hydrol. **505**: 47–64. doi:10.1016/j.jhydrol.2013.09.006

Liao, Z., L. Bao, M. Fan, P. Gao, X. Wang, C. Qin, and X. Li. 2015. In-depth proteomic analysis of nacre, prism, and myostracum of *Mytilus* shell. J. Proteomics **122**: 26–40. doi:10.1016/j.jprot.2015.03.027

Marin, F., N. Le Roy, and B. Marie. 2012. The formation and mineralization of mollusk shell. Front. Biosci. **S4**: 1099–1125. doi:10.2741/s321

McConnaughey, T. A. 1989. ^{13}C and ^{18}O isotopic disequilibrium in biological carbonates: II. *In vitro* simulation of kinetic isotope effects. Geochim. Cosmochim. Acta **53**: 163–171. doi:10.1016/0016-7037(89)90283-4

McConnaughey, T. A., and D. P. Gillikin. 2008. Carbon isotopes in mollusk shell carbonates. Geo-Mar. Lett. **28**: 287–299. doi:10.1007/s00367-008-0116-4

Mook, W. G., and J. C. Vogel. 1968. Isotopic equilibrium between shells and their environment. Science **159**: 874–875. doi:10.1126/science.159.3817.874

Mutvei, H., and T. Westermark. 2001. How environmental information can be obtained from naiad shells. Ecol. Stud. **145**: 367–379. doi:10.1007/978-3-642-56869-5_21

Nakahara, H., and G. Bevelander. 1971. The formation and growth of the prismatic layer of *Pinctada radiata*. Calcif. Tissue Res. **7**: 31–45. doi:10.1007/BF02062591

Namikawa, Y., K. Moriyasu, K. Yasumoto, S. Katsumata, and M. Suzuki. 2023. Carbonic anhydrase activity identified in the powdered nacreous layer of *Pinctada fucata*. Process Biochem. **128**: 22–29. doi:10.1016/j.procbio.2023.02.007

Owen, R., H. Kennedy, and C. Richardson. 2002. Isotopic partitioning between scallop shell calcite and seawater: Effect of shell growth rate. Geochim. Cosmochim. Acta **66**: 1727–1737. doi:10.1016/S0016-7037(01)00882-1

Pfister, L., F. Thielen, E. Deloule, N. Valle, E. Lentzen, C. Grave, J.-N. Beisel, and J. J. McDonnell. 2018. Freshwater pearl mussels as a stream water stable isotope recorder. Ecohydrology **11**: e2007. doi:10.1002/eco.2007

Pfister, L., C. Grave, J.-N. Beisel, and J. J. McDonnell. 2019. A global assessment of freshwater mollusk shell oxygen isotope signatures and their relation to precipitation and stream water. Sci. Rep. **9**: 4312. doi:10.1038/s41598-019-40369-0

Sade, Z., and I. Halevy. 2017. New constraints on kinetic isotope effects during CO_2(aq) hydration and hydroxylation: Revisiting theoretical and experimental data. Geochim. Cosmochim. Acta **214**: 246–265. doi:10.1016/j.gca.2017.07.035

Sakoe, H., and S. Chiba. 1978. Dynamic programming algorithm optimization for spoken word recognition. IEEE Trans. Acoust. Speech Signal Process. **26**: 43–49. doi:10.1109/TASSP.1978.1163055

Schöne, B. R., M. Pfeiffer, T. Pohlmann, and F. Siegismund. 2005. A seasonally resolved bottom-water temperature record for the period AD 1866-2002 based on shells of *Arctica islandica* (Mollusca, North Sea). Int. J. Climatol. **25**: 947–962. doi:10.1002/joc.1174

Schöne, B. R., A. E. Meret, S. M. Baier, J. Fiebig, J. Esper, J. McDonnell, and L. Pfister. 2020. Freshwater pearl mussels from northern Sweden serve as long-term, high-resolution stream water isotope recorders. Hydrol. Earth Syst. Sci. **24**: 673–696. doi:10.5194/hess-24-673-2020

Trofimova, T., S. Milano, C. Andersson, F. G. W. Bonitz, and B. R. Schöne. 2018. Oxygen isotope composition of *Arctica islandica* aragonite in the context of shell architectural organization: Implications for paleoclimate reconstructions. Geochem. Geophys. Geosyst. **19**: 453–470. doi:10.1002/2017GC007239

Trofimova, T., and others. 2020. Fundamental questions and applications of sclerochronology: Community-defined research priorities. Estuar. Coast. Shelf Sci. **245**: 106977. doi:10.1016/j.ecss.2020.106977

Versteegh, E. A. A., H. B. Vonhof, S. R. Troelstra, R. J. G. Kaandorp, and D. Kroon. 2010. Seasonally resolved growth of freshwater bivalves determined by oxygen and carbon isotope shell chemistry. Geochem. Geophys. Geosyst. **11**. doi:10.1029/2009GC002961

Waite, A. J., and P. K. Swart. 2015. The inversion of aragonite to calcite during the sampling of skeletal archives: Implications for proxy interpretation. Rapid Commun. Mass Spectrom. **29**: 955–964. doi:10.1002/rcm.7180

Wang, K., and T. Gasser. 1997. Alignment of curves by dynamic time warping. Ann. Stat. **25**: 1251–1276. doi:10.1214/aos/1069362747

Wefer, G., and W. H. Berger. 1991. Isotope paleontology: Growth and composition of extant calcareous species. Mar. Geol. **100**: 207–248. doi:10.1016/0025-3227(91)90234-U

Zeebe, R. E., and D. Wolf-Gladrow. 2001. *CO_2 in seawater: Equilibrium, kinetics, isotopes*. Gulf Professional Publishing.

Acknowledgments

We thank Michael Maus (JGU Mainz) for isotope measurements and Alessandro Aiello (JGU Mainz) as well as Tom Neder (JGU Mainz) for laboratory assistance. We are grateful for the thorough reading of the manuscript by two anonymous reviewers and the guest editor (Clive Trueman). Their comments significantly enhanced the clarity of the manuscript. Open Access funding enabled and organized by Projekt DEAL.

Submitted 16 January 2024
Revised 11 July 2024
Accepted 17 July 2024